ISSN 1063-7761, Journal of Experimental and Theoretical Physics, 2023, Vol. 137, No. 6, pp. 903–913. © Pleiades Publishing, Ltd., 2023.
Russian Text © The Author(s), 2023, published in Zhurnal Eksperimental'noi i Teoreticheskoi Fiziki, 2023, Vol. 164, No. 6, pp. 1026–1038.

ORDER, DISORDER, AND PHASE TRANSITION IN CONDENSED SYSTEM

Magnetic Interparticle Interactions and Superparamagnetic Blocking of Powder Systems of Biogenic Ferrihydrite Nanoparticles

A. A. Krasikov[a,*], Yu. V. Knyazev[a], D. A. Balaev[a,], S. V. Stolyar[a,b], V. P. Ladygina[b], A. D. Balaev[a], and R. S. Iskhakov[a]**

[a] *Kirensky Institute of Physics, Siberian Branch, Russian Academy of Sciences, Akademgorodok, Krasnoyarsk, 660036 Russia*

[b] *Federal Research Center "Krasnoyarsk Science Center of the Siberian Branch of the Russian Academy of Sciences," Krasnoyarsk, 660036 Russia*

**e-mail: KAA3000@yandex.ru*

***e-mail: dabalaev@iph.krasn.ru*

Received July 10, 2023; revised July 26, 2023; accepted July 27, 2023

Abstract—The magnetic-field dependence of the superparamagnetic-blocking temperature T_B of systems of antiferromagnetically ordered ferrihydrite nanoparticles has been investigated and analyzed. We studied two powder systems of nanoparticles: particles of "biogenic" ferrihydrite (with an average size of 2.7 nm), released as a result of vital functions of bacteria and coated with a thin organic shell, and particles of biogenic ferrihydrite subjected to low-temperature annealing, which cause an increase in the average particle size (to 3.8 nm) and burning out of the organic shell. The character of the temperature dependences of magnetization, measured after cooling in a weak field, as well as the shape of the obtained dependences $T_B(H)$, demonstrate peculiar features, indicating the influence of magnetic interparticle interactions. A detailed analysis of the dependences $T_B(H)$ within the random magnetic anisotropy model made it possible to estimate quantitatively the intensity of magnetic particle–particle interactions and determine the magnetic anisotropy constants of individual ferrihydrite particles.

DOI: 10.1134/S1063776123120075

1. INTRODUCTION

Studies of the magnetic properties of powder systems of magnetic nanoparticles are an integral part of their characterization; such studies make it possible to determine the parameters that are important both from the point of view of physical materials science and for specific applications. These parameters include the particle magnetic moment and the effective (depending on the particle size) magnetic anisotropy constant K_{eff}. However, one should distinguish between the properties of an individual nanoparticle and the properties of an ensemble of nanoparticles. For the latter, of great importance may be the effects of magnetic interparticle interactions; if they are ignored, the experimentally found values of parameters may be incorrect. This can be illustrated, for example, by consideration of the temperature T_B of superparamagnetic (SPM) blocking (which is generally determined from the magnetic susceptibility or magnetization in a weak field after cooling in zero external field (zero field cooling, ZFC)). For systems of noninteracting particles the temperature T_B is defined as

$$T_B = K_{eff}V / \ln(\tau_m/\tau_0)k. \quad (1)$$

This relation follows from the Néel–Brown expression for the characteristic time τ of the particle magnetic moment flip,

$$\tau = \tau_0 \exp(K_{eff}V/kT)$$

at $\tau = \tau_m$ (τ_m is the characteristic time of the experimental technique, V is the particle volume, τ_0 ranges from 10^{-9} to 10^{-13} s, and k is the Boltzmann constant). According to the numerous experimental data [1–7], concerning systems of nanoparticles with identical sizes, the temperature T_B may significantly increase for the systems characterized by magnetic particle–particle interactions. In this case, estimation according to expression (1) will yield an overestimated value of K_{eff}.

There are different approaches to the detection and estimation of the degree of influence of magnetic interparticle interactions on physical parameters [1, 4, 8–12]. One of them, proposed for the first time in [3, 8], is based on the analysis of the field dependence of the SPM blocking temperature. In this study this approach is applied to powder systems of ferrihydrite nanoparticles.

Ferrihydrite (described by the nominal chemical formula $Fe_2O \cdot nH_2O$) belongs to the class of antiferromagnetic (AFM) materials [13]. These materials, implemented in the form of nanoparticles, demonstrate magnetic characteristics similar to those of ferro- or ferrimagnetic (FM) oxide nanoparticles [13, 14]. The foundation of the physics of nanoscale AFM particles was laid by Néel [15]; the incomplete compensation of magnetic sublattices in nanoparticles can be considered as the main difference of AFM nanoparticles from their bulk analogs. This feature leads to the occurrence of an uncompensated magnetic moment μ_{un} in AFM nanoparticles, which can be estimated from the relation

$$\mu_{un} \sim \mu_{at} N^b. \quad (2)$$

Here, μ_{at} is the magnetic moment of a magnetoactive atom, N is the number of magnetoactive atoms per particle, and the exponent b depends on the type of the defects leading to decompensation; it may take values in the range of 1/3–2/3 [15].

Expression (2) predicts a fairly small value of μ_{un} for AFM particles with N on the order of 10^4–10^5 (the particle size is several tens of nanometers) as compared with the magnetic moment μ_p of FM nanoparticles. However, for particles of extremely small sizes (2–4 nm, i.e., specifically the range characteristic of ferrihydrite), the μ_{un} value becomes comparable with μ_p for FM particles (for the latter, the large surface fraction negatively affects the μ_p value because of the formation of a magnetically dead surface layer [16–19]). For ferrihydrite nanoparticles and ferritin molecules, it was found that μ_{un} is formed by spins of several tens of iron atoms in a particle ($\mu_{at} \approx 5\ \mu_B$, where μ_B is the Bohr magneton) and reaches values of 100–300 μ_B (the exponent b in expression (1) is $\approx 1/2$) [20–26].

Ferrihydrite can be obtained either chemically [22, 27, 28] or as a product of vital functions of bacteria or microorganisms [24, 29]. In the former case, the powder system consists of nanoparticles directly contacting each other. However, biogenic ferrihydrite allows partial formation of an ultrathin organic coating of particles [29, 30], caused by bacteria cultivation conditions. One of few efficient ways to control the sizes of ferrihydrite nanoparticles is the low-temperature (150–200°C) heat treatment of the obtained sol [25, 26, 31, 32]. The increase of particles in size during this low-temperature heat treatment is related to their agglomeration; in the case of biogenic ferrihydrite, this process is also accompanied by "burning out" of the organic shell. Note that ferrihydrite is transformed into hematite at higher annealing temperatures [32–34].

A significant influence of magnetic interparticle interactions on the magnetic properties of powder ferrihydrite systems was noted in several studies [30, 35–40] based on the analysis of data on the AC magnetic susceptibility or the Mössbauer effect. It appears interesting to perform a similar analysis by considering the field dependence of the SPM blocking temperature. Our purpose was to establish the role of magnetic interparticle interactions in implementation of the SPM state of biogenic ferrihydrite nanoparticles. To this end, we investigated and analyzed (within the model [3, 8]) the dependences $T_B(H)$ for two samples: initial sample of biogenic ferrihydrite and sample subjected to low-temperature annealing.

2. EXPERIMENTAL

A biogenic ferrihydrite sample was obtained by isolation from bacterial precipitates after cultivation of *Klebsiella oxytoca* bacteria under anaerobic conditions, as described previously in [24, 31, 37]. The product (a dried sol) is an aggregated system of ferrihydrite nanoparticles with a small average size of ~2–3 nm, coated with a thin organic shell [30]. The biogenic ferrihydrite sample under study will be denoted below as FH-0h. A part of this sample was subjected to low-temperature annealing at 150°C in air for 24 h. Below this sample will be denoted as FH-24h.

An electron microscopy study was performed on a Hitachi HT7700 transmission electron microscope at an accelerating voltage of 100 kV. Samples were prepared by shaking nanoparticle powder in alcohol in an ultrasonic bath, with subsequent deposition of the obtained suspension on supporting grids with a perforated carbon coating.

Mössbauer spectra were obtained on an MS-1104Em spectrometer (developed at the Research Institute of Physics of the Southern Federal University, Russia) with a Co^{57}(Rh) source in the temperature range of 4–300 K using a CFSG-311-MESS cryostat (Cryotrade Engineering).

Temperature dependences of the magnetization $M(T)$ were measured on a SQUID magnetometer [41] in a field $H = 100$ Oe and on a vibrational magnetometer [42] in stronger fields (1–30 kOe). Modes of cooling in zero external field (zero field cooling (ZFC)) and in external field (field cooling (FC)) were used. The magnetic moment data are given in emu units per studied powder mass.

3. CHARACTERIZATION

3.1. Microstructure

Figure 1 presents typical transmission electron microscopy (TEM) data on the investigated samples. One can visually see in the micrographs that the particle size in sample FH-24h is larger than in the initial sample FH-0h. This is confirmed by the particle size distributions (plotted based on several micrographs) in Fig. 1. The average particle sizes $\langle d \rangle$ turned out to be 2.7 and 3.8 nm, and the maximum sizes of detected particles, d_{max}, were 3.3 and 5.8 nm for samples FH-0h and FH-24h, respectively. Note that it is fairly prob-

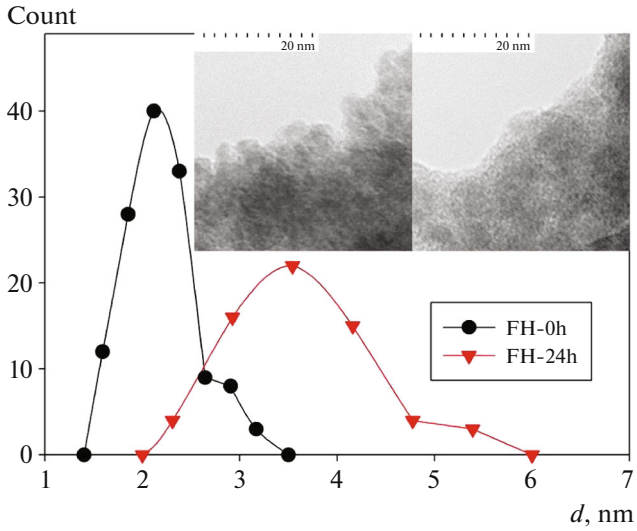

Fig. 1. Typical TEM images of samples FH-0h and FH-24h (on the left and right, respectively) and the particle size distributions.

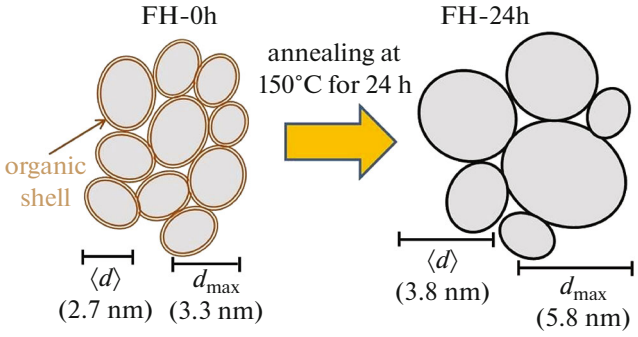

Fig. 2. Schematic of the microstructure transformation as a result of annealing for samples FH-0h and FH-24h, with preservation of the relative sizes of ferrihydrite nanoparticles.

lematic to establish the presence (or absence) of organic coating on ferrihydrite particles based on TEM data. The aforementioned d_{max} values will be used when analyzing the dependences $T_B(H)$. The increase in the particle size after the low-temperature annealing is related to the organic shell "burn out" in the initial sample and further agglomeration of particles, leading to their coarsening. This process is schematically shown in Fig. 2, with relative particle sizes preserved.

3.2. Mössbauer Spectroscopy

The Mössbauer spectra of the investigated samples at $T = 4.2$ and 300 K are shown in Fig. 3. The spectra of the samples at room temperature (Fig. 3a) present a doublet, described by a superposition of three components. The values of the Mössbauer parameters, including the isomer shift IS and quadrupole splitting QS (see Table 1), are in good agreement with the known data on ferrihydrite [33, 38, 43, 44]. The three aforementioned components correspond to three nonequivalent iron sites (denoted as Fe1, Fe2, Fe3) in ferrihydrite [33, 38, 43, 44]. Iron cations are in the trivalent state in all sites. The ratio of the relative occupancies A of these doublets in the spectra of both samples is practically the same and close to 3 : 2 : 1. As applied to nanoscale magnetic particles, the aforementioned doublet is a manifestation of the SPM state of the magnetic moments of particles [13, 37, 38, 45].

A decrease in temperature leads to the occurrence of a hyperfine structure in the spectrum (Fig. 3b); this is a sign of a blocked state of particle magnetic moments in Mössbauer spectroscopy [13, 37, 38, 45]. In our case, we speak about uncompensated magnetic moments μ_{un} of particles (see Introduction). Mathematical processing of the spectra recorded at $T = 4.2$ K, as well as for the spectra obtained at $T = 300$ K), shows the existence of three characteristic iron sites (Fe1, Fe2, Fe3) in an octahedral coordination. The relative occupancies A of the Fe1, Fe2, and Fe3 sites coincide (within the processing error) with the data on the spectra recorded at $T = 300$ K. It can be seen in Table 2 that the hyperfine field H_{hf} for sample FH-24h somewhat exceeds that for sample FH-0h. This is most likely due to the larger particle size in sample FH-24h (see Figs. 1, 2).

Thus, the Mössbauer spectroscopy data confirm that both samples are aggregates of ferrihydrite nanoparticles. Low-temperature annealing did not produce any other iron oxide phases.

Table 1. Mössbauer parameters at temperatures of 4.2 and 300 K. IS is the isomer shift relative to α-Fe, ±0.005 mm/s; H_{hf} is the hyperfine field on iron nuclei, ±2 kOe; QS is the quadrupole splitting, ±0.02 mm/s; W is the width of the Mössbauer line at the half height, ±0.02 mm/s; and A is the relative site occupancy, ±0.05 au

Sample/T	IS	H_{hf}	QS	W	A	Site
FH-24h	0.336	–	0.52	0.37	0.51	Fe1
300 K	0.338	–	0.87	0.35	0.37	Fe2
	0.338	–	1.27	0.33	0.13	Fe3
FH-24h	0.488	513	0.0	0.49	0.45	Fe1
4.2 K	0.458	489	0.0	0.58	0.30	Fe2
	0.428	459	0.0	0.49	0.23	Fe3
FH-0h	0.334	–	0.47	0.37	0.48	Fe1
300 K	0.343	–	0.74	0.29	0.30	Fe2
	0.344	–	1.06	0.33	0.22	Fe3
FH-0h	0.501	508	0.0	0.23	0.47	Fe1
4.2 K	0.480	479	0.0	0.33	0.36	Fe2
	0.499	443	0.0	0.58	0.15	Fe3

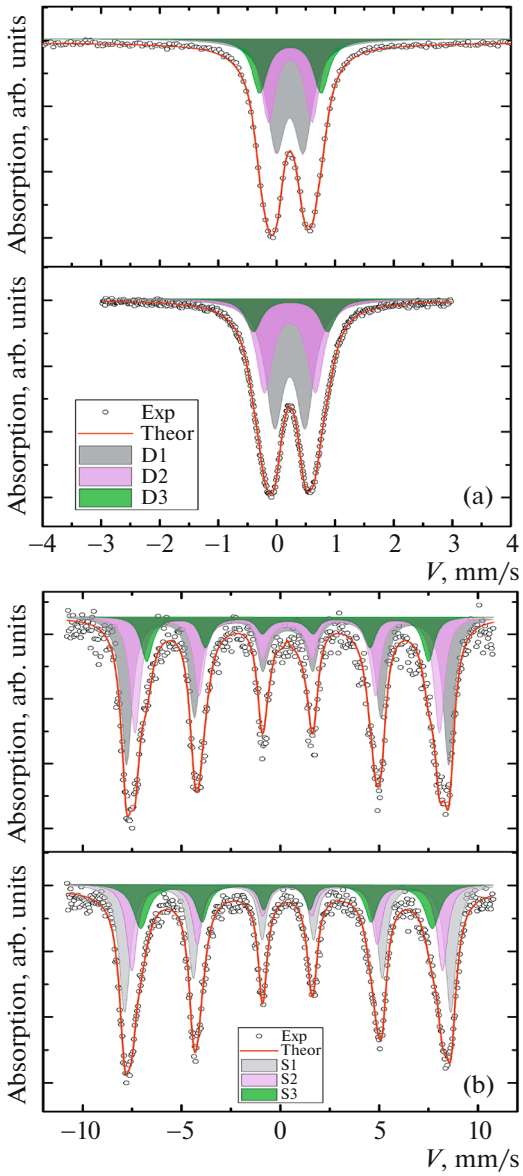

Fig. 3. Mössbauer spectra of samples FH-0h (top) and FH-24h (bottom), recorded at (a) 300 and (b) 4.2 K. Symbols are experimental data, and solid lines are processing results; filled doublets D (a) and sextets S (b) are partial spectral components (the numbers for D1–D3 and S1–S3 correspond to the iron sites Fe1–Fe3, respectively; see Table 1).

4. RESULTS AND DISCUSSION

Figure 4 illustrates the dependences $M(T)$ for the investigated samples, obtained in different external fields and in the ZFC and FC modes. The data for each field contain at least two characteristic points: the temperature of irreversible behavior of magnetization, T_{irr} (in the range $T > T_{irr}$ the dependence $M(T)_{ZFC}$ and $M(T)_{FC}$ coincide) and the temperature T_{max}, at which the dependences $M(T)_{ZFC}$ demonstrate a maximum. Both temperatures, T_{irr} and T_{max}, decrease with an increase in the external field. The above-described behavior is typical of systems of magnetic nanoparticles in which the transition from the SPM state (high temperatures) to the blocked state (low temperatures) occurs. The larger T_{irr} and T_{max} values (in the same field) for sample FH-24h can reasonably be explained in terms of expression (1), taking into account the fact that the particle size in sample FH-24h is noticeably larger than that in sample FH-0h (see Subsection 3.1 and Figs. 1, 2). In fields $H \geq 1$ kOe the dependences $M(T)_{FC}$ for both samples have a "classical" form: the magnetization increases with a decrease in temperature in the temperature range below T_{max}. However, in the field $H = 100$ Oe for sample FH-0h the dependence $M(T)_{FC}$ in the vicinity of $\langle T_{max} \rangle$ is a weakly changing function, demonstrating a weak local minimum (see inset in Fig. 4a).This form of the dependence $M(T)$ under the FC conditions is a characteristic sign of the presence of magnetic interparticle interactions [2–5, 29, 38, 40]. For sample FH-24h, the dependence $M(T)_{FC}$ in the vicinity of $\langle T_{max} \rangle$ is a function decreasing with increasing temperature (see inset in Fig. 4b), which may indicate indirectly to a stronger influence of magnetic interparticle interactions. Therefore, we will analyze the obtained data (specifically, the field dependences of SPM blocking temperatures) within the model [8], taking into account these interactions.

The model developed in [3, 8], called as the random anisotropy model by the authors (RA model below), is based on the consideration of a cluster of particles, in which the behavior of the magnetic moments of particles is correlated because of the influence of magnetic interparticle interactions. Then, expression (1), which determines the SPM transition temperature, will include an "effective" volume of a cluster containing several particles instead of the volume V of one particle (for example, of a medium-size particle). With an increase in the external field the cluster size should decrease, because the Zeeman energy $\mu_p H$ will exceed the energy of magnetic interparticle interactions, and the influence of the latter will be weak. Then, in a sufficiently strong external field, the "effective" cluster size will be close to the particle size, and the SPM blocking temperature will take approximately the same value as for a system of noninteracting particles. The following field dependence of the cluster size $L_H(H)$ was proposed in [3, 8]:

$$L_H(H) = d + \sqrt{\frac{2A_{eff}}{M_S H + C}}. \quad (3)$$

Here, M_S is the particle saturation magnetization, and the parameters A_{eff} and C characterize the intensity of magnetic particle–particle interactions. Expression (3) contains a root dependence of the correlation length on external field, which follows from the micromagnetic theory [46], and A_{eff} has the same meaning as the

Table 2. Parameters used to plot the dependences $T_{irr}(H)$ in Fig. 5b and the ratios $L_H(H=0)/\langle d\rangle$ ($\langle d\rangle = 2.7$ and 3.8 nm for samples FH-0h and FH-24h, respectively)

Sample	x	K_{eff}, erg/cm^3	C, erg/cm^3	A_{eff}, erg/cm	$L_H(H=0)$, nm	$\frac{L_H(H=0)}{\langle d\rangle}$
FH-0h	0.75	2.1×10^6	11.7×10^4	100×10^{-10}	7.4	2.7
FH-24h	1	$1{,}4 \times 10^6$	4.8×10^4	120×10^{-10}	13.0	3.4

exchange constant for nanocrystalline alloys [3, 8]; obviously, this value is proportional to the intensity of magnetic interparticle interactions. The parameter C also characterizes the interparticle interactions; it is inversely proportional to their force. Mathematically, this parameter eliminates the divergence of expression (3) in weak external fields; at large C values the concept of correlation length L_H loses sense: $L_H \approx d$. For the particle cluster under consideration, the magnetic anisotropy constant K_H will differ from that for an individual particle: $K_H = K_{eff}/N_P^{1/2}$, where N_P is the number of particles per cluster, and K_{eff} corresponds to the characteristic of an individual noninteracting particle [3, 8] (as in expression (1)).

The classical dependence $T_B(H)$ for noninteracting particles, along with the factor $T_B(H=0)$ (expression (1)), is determined by a power-law function of the external field [3, 8]:

$$T_B(H) = \frac{K_{eff}V}{k_B \ln(\tau/\tau_0)}\left[1 - \frac{M_S H}{2K_{eff}}\right]^{3/2}. \quad (4)$$

Substitution of the cluster volume instead of a particle volume (in the case of spherical particles) and the corresponding anisotropy constant K_H into (4), with allowance for the volume concentration x of magnetic particles, leads to the following expression for the SPM blocking temperature:

$$T_B(H) = \frac{\pi K_{eff}[d^3 + x(L_H^3 + d^3)]}{6k_B \ln\left(\frac{\tau_m}{\tau_0}\right)\sqrt{1 + \frac{x(L_H^3 - d^3)}{d^3}}} \times \left[1 - \frac{M_S H\sqrt{1 + \frac{x(L_H^3 - d^3)}{d^3}}}{2K_{eff}}\right]^{\frac{3}{2}}. \quad (5)$$

According to expressions (1) and (5), the SPM blocking temperature is proportional to the volume of particles. Obviously, the temperature T_{irr}, characterizing the onset of the irreversible behavior of the dependences $M(T)$ (Fig. 4), corresponds to the particles of maximum size, d_{max}. On the other hand, it is sometimes expedient to consider the function $f_d(T) = -(d(M(T)_{FC} - M(T)_{ZFC}/dT))$ [4, 8, 31]. The temperature at which the function $f_d(T)$ reaches a maximum is identified with the SPM blocking temperature $\langle T_B\rangle$ of mean-size $\langle d\rangle$ particles. However, within this approach for the data at $H = 30$ kOe (for sample FH-24h), and $H = 10$ kOe or more (for sample FH-0h), the temperature $\langle T_B\rangle$ is already beyond the experimentally available range: below 4.2 K. In addition, in a sufficiently weak field ($H = 100$ Oe), the dependence $f_d(T)$

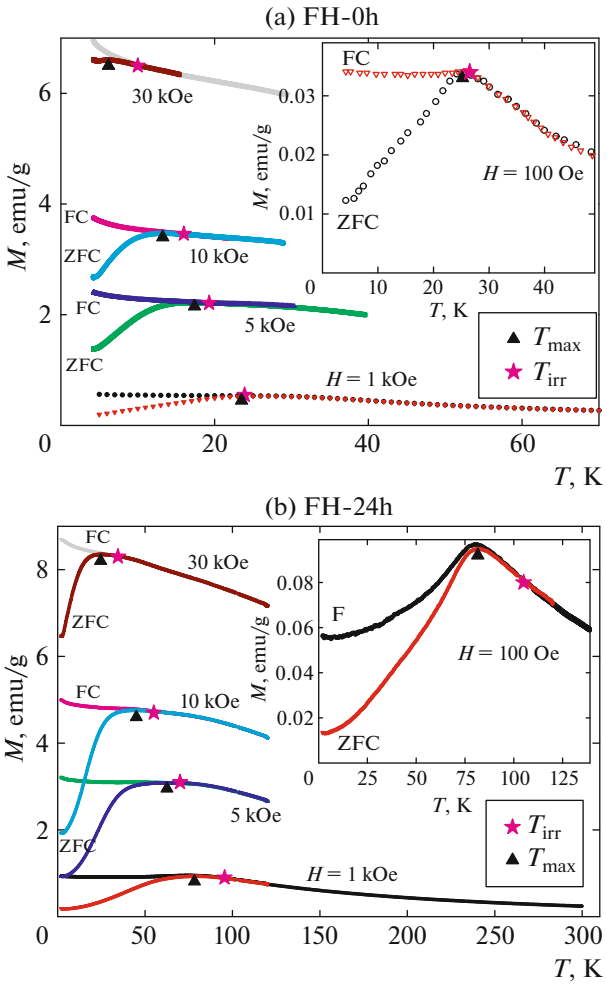

Fig. 4. Temperature dependences of the magnetization $M(T)_{ZFC}$ and $M(T)_{FC}$ in different fields (indicated) for samples (a) FH-0h and (b) FH-24h. The insets show the data for $H = 100$ Oe. The characteristic temperatures of irreversible behavior of magnetization (T_{irr}) and maximum in the dependence $M(T)_{ZFC}$ (T_{max}) are also shown (see legends).

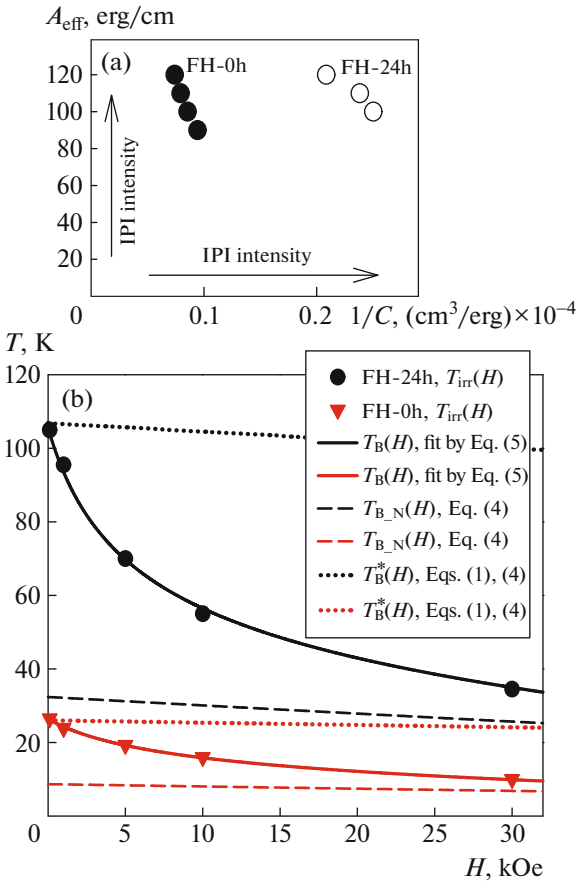

Fig. 5. (a) Ranges of the values of fitting parameters C and A_{eff} at which good agreement between dependences $T_{irr}(H)$ and calculation according to the RA model, in the coordinates $1/C$–A_{eff}, is obtained. (b) Dependences of the temperature T_{irr} on the external field H (symbols) for the investigated samples. Solid lines are the results of fitting within the RA model: expressions (3) and (5) with the parameters listed in Table 2. Dotted lines are plotted according to expression (4) in accordance with the experiment in a field of 100 Oe. Dashed lines are the "expected" dependences of blocking temperature in complete absence of magnetic interparticle interactions (expression (4)) with the K_{eff} values given in Table 2.

for sample FH-24h is a complex nonmonotonic function, and it is impossible to determine the $\langle T_B \rangle$ value. The temperature $\langle T_{max} \rangle$ for the dependences $M(T)_{ZFC}$ corresponds to the blocking of particles of a certain size, located in the range between $\langle d \rangle$ and d_{max}; however, in this case, there is an uncertainty in the choice of this size. Based on these considerations, carrying out further analysis of the influence of external field on the SPM blocking temperature, we will use the characteristic temperature T_{irr}, assuming that it corresponds to the maximum particle size d_{max}. Note that processing of the existing data $\langle T_B \rangle$ from the functions $f_d(T)$ yields similar results.

The experimental dependences $T_{irr}(H)$ are shown in Fig. 5b (symbols). To analyze the dependence $T_{irr}(H)$ within the RA model [3, 8] (expressions (3) and (5)), one must determine the minimum number of fitting parameters.

The M_S values are determined by analyzing the isotherms of the magnetization curves $M(H)$ in the range of SPM temperatures [13, 14]. Generally this analysis implies fitting of experimental data by a function of the $M(H) = M_{SP}(H) + \chi H$ type. The first term in this function is responsible for the SPM behavior of uncompensated magnetic moments of particles (μ_{un}), and the second term corresponds to the AFM susceptibility and other contributions, linearly depending on the external field [20–27, 29, 37, 38, 48, 49]. As a result of fitting, with allowance for the distribution $f(\mu_{un})$, the mean magnetic moment of a particle, $\langle \mu_{un} \rangle$, is determined; the $\langle \mu_{un} \rangle$ values generally change only slightly in the low-temperature range [20–27, 29, 37, 38, 48, 49]. The $\langle \mu_{un} \rangle$ values for samples FH-0h and FH-24h in the low-temperature region are, respectively, $\approx 160\mu_B$ and $\approx 300\mu_B$. Using the relation $M_S = \mu_{un}/V$, we find the M_S values to be 20 and 13.3 Gs (at a physical ferrihydrite density of ≈ 3.8 g/cm^3) for samples FH-0h and FH-24h, respectively. These M_S values were used to fit the dependences $T_{irr}(H)$; a variation in these values within $\pm 5\%$ barely affects the results of the analysis.

The particle concentration x is determined by the thickness of the organic coating of ferrihydrite particles, which, according to the results of [30], is present in sample FH-0h. We take x to be 0.75 for this sample, proceeding from the reasonable assumption of a fairly thin coating with an average thickness of about 0.15 nm. Low-temperature annealing leads to coarsening of ferrihydrite nanoparticles; the most significant changes occur after several hours of annealing [26, 27], whereas the difference in the magnetic properties for the samples annealed for 24 and 240 h is small [26, 27]. This fact suggests that, during annealing for about 24 h, the organic shell almost completely "burns out;" therefore, we took $x = 1$ for sample FH-24h. A variation in the aforementioned x values within ± 0.1 leads to a change in other fitting parameters by no more than 5–7%.

For the characteristic times τ_m and τ_0 in expressions (3) and (5), we used the generally accepted values of 10^2 s and 10^{-12} s, respectively [13], and the maximum particle sizes d_{max} corresponded to the TEM data (Subsection 3.1): 3.3 and 5.8 nm for samples FH-0h and FH-24h, respectively.

Thus, three variable parameters remain in expressions (3) and (5): K_{eff}, A_{eff}, and C. The first of them may somewhat differ for particles of different sizes because of the contribution of surface magnetic anisotropy [50, 51]. However, the K_{eff} value in expression (5) affects mainly the SPM blocking temperature in sufficiently strong fields. The other two parameters, A_{eff} and C, determine the field dependence of the clus-

ter size $L_H(H)$, and the fitting procedure is reduced to determination of the functional dependence $L_H(H)$ at which the experimental data (dependence $T_{irr}(H)$) are adequately described. A larger value of A_{eff} unambiguously corresponds to an increase in the size L_H, whereas a smaller C value leads to a rise in L_H in weak fields.

Therefore, the points corresponding to the C and A_{eff} values, obtained by processing experimental data, in the $1/C$–A_{eff} coordinates should move from left to right and upwards with enhancement of magnetic interparticle interactions. The ranges of the discussed parameters at which good agreement is obtained are shown (in the aforementioned coordinates) in Fig. 5a. Although the ranges of A_{eff} values are close for the investigated samples, the tendency of motion from left to right and upwards is observed for the sample with particles free of organic shell. Note that, at some arbitrary choice of a specific pair of fitting parameters in Fig. 5a, the correlation length L_H (see below) barely changes. Figure 5b shows typical results of processing the dependences $T_{irr}(H)$ within the above-described approach. The parameters x, K_{eff}, C, and A_{eff}, used to construct the dependences $T_{irr}(H)$ in Fig. 5b based on expressions (3) and (5), are listed in Table 2.

It is of interest to compare the results of the above analysis within the RA model with the approach where the magnetic particle–particle interactions are disregarded. Figure 5b shows the field dependences of SPM blocking temperature, calculated from expression (4) and denoted as $T_B^*(H)$ (dotted lines in Fig. 5b). The K_{eff}^* values at which the values $T_B^*(H = 0)$ are in agreement with the experimental T_{irr} values in a weak external field (100 Oe) were used for these dependences. In this case the K_{eff} values are three or even more times larger than those obtained within the RA model (compare with the data of Table 2): $K_{eff}^* \approx 6.15 \times 10^6$ erg/cm^3 for sample FH-0h and $K_{eff}^* \approx 4.65 \times 10^6$ erg/cm^3 for sample FH-24h. One can also calculate the "expected" field dependences of the SPM blocking temperature for the case where particles in the investigated samples are spatially separated so that the magnetic interactions between them are negligible. To plot these dependences, denoted below as $T_{B\_N}(H)$, we took the K_{eff} values yielded by the RA model (Table 2) and used expression (4) with the same values $d = d_{max}$. These dependences are shown by dashed lines in Fig. 5b. The difference between T_B^* and T_{B_N} in a weak external field is ≈75 K for sample FH-24h (at $T_B^*(0) \approx T_{irr}$ (100 Oe) ≈ 107 K) and ≈17.4 K for sample FH-0h (at $T_B^*(0) \approx T_{irr}$ (100 Oe) ≈ 26.3 K). These estimates prove convincingly that, when determining such an important parameter as the magnetic anisotropy constant for systems of ferrihydrite nanoparticles, the use of the data on SPM blocking temperature obtained in weak fields leads to overestimated values.

Let us now consider the K_{eff} values obtained within the RA model. It can be seen in Table 2 that the K_{eff} value is smaller for larger particles. This is obviously related to the influence of surface magnetic anisotropy, because the magnetic interactions between particles are already taken into account here. The contribution of the surface magnetic anisotropy is generally related to the corresponding constant K_S; it is recorded, with allowance for the constant of volume magnetic anisotropy K_V, in the form [50, 51]

$$K_{eff} = K_V + 6K_S/d. \quad (6)$$

Substituting the K_{eff} values and the corresponding values $d = d_{max}$ into expression (6), one can find that $K_V \approx 4.7 \times 10^5$ erg/cm^3 and $K_S = 0.09$ erg/cm^2. The found K_S value is typical of iron oxide nanoparticles [52–58] and close to the values obtained for other nanoferrihydrite samples[1] [29, 37, 38].

Let us analyze the parameters obtained within the RA model, which describe the intensity of magnetic interactions. Both parameters, A_{eff} and C, determine the correlation length L_H. Table 2 contains the $L_H(H = 0)$ values, and the field dependences $L_H(H)$ are shown in Fig. 6. The correlation length for sample FH-24h is larger than for sample FH-0h; however, these samples differ in the particle size (Figs. 1, 2). For comparison with the dependences $L_H(H)$, Fig. 6 presents also the maximum (d_{max}) and mean $\langle d \rangle$ particle sizes (horizontal lines). It can be seen in Fig. 6 that the L_H value decreases with an increase in the external field, approaching d_{max} in fields of about 30 kOe, in correspondence with the concept of the RA model.

It is reasonable to consider the ratio $L_H(H)/d$ as one of the characteristics of magnetic interaction intensity. This value shows how many times the L_H in an external field exceeds the particle size d. Table 2 contains the $L_H/\langle d \rangle$ values for zero external field; their comparison shows that the influence of interparticle interactions is stronger for sample FH-24h, although the $L_H(H = 0)/\langle d \rangle$ values differ by only 20–25%. For sample FH-0h at $H \approx 0$, a cluster of size L_H contains $2.7^3 \approx 20$ particles of mean size, whereas in sample FH-24h at $H \approx 0$ such a cluster contains about $3.4^3 \approx 40$ particles of mean size. In a sufficiently strong external field, $H = 30$ kOe, there are 7–8 mean-size particles per cluster in both samples.

Based on the above analysis, one can say that the contribution of magnetic interparticle interactions to SPM blocking processes occurs in both samples, but the influence of these interactions is more pronounced for sample FH-24h. Estimation of the energy

[1] The K_{eff} values according to expression (5) were obtained in the approximation of spherical particles, while expression (6) may be more valid for cubic particles.

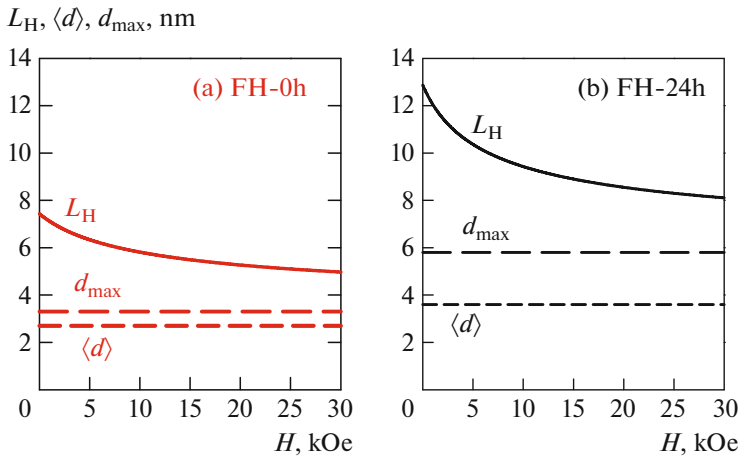

Fig. 6. Dependence of the cluster size L_H on external field, obtained by fitting the dependences $T_{irr}(H)$ (Fig. 5b) according to expressions (3) and (5), in comparison with the mean $\langle d \rangle$ and maximum (d_{max}) particle sizes in samples (a) FH-0h and (b) FH-24h.

of magnetic dipole–dipole interactions $E_{dip} = T_{dip}$ can only qualitatively explain the influence of magnetic interparticle interactions for both samples. According to the estimates obtained in the Appendix, E_{dip} is ≈7 K for sample FH-0h and ≈12.3 K for sample FH-24h (this is the upper limit for the aforementioned estimates). It was also shown in the Appendix that E_{dip} should be practically independent of the particle size in the case of ferrihydrite, and the large E_{dip} value for sample FH-24h is determined by the absence of organic shell on particles in this sample. The aforementioned E_{dip} values (≈7 K for sample FH-0h and ≈12.3 K for sample FH-24h) cannot quantitatively explain the difference between the experimental T_{irr} values and estimated T_{B_N} values (obtained from the K_{eff} value in Table 2) in a weak external field (see Fig. 5b). It was shown above that the difference $T_{irr} - T_{B\_N}$ is ≈17.4 K and ≈75 K in a field $H = 100$ Oe for samples FH-0h and FH-24h, respectively.

Thus, we can conclude that magnetic interparticle interactions are caused by either exchange (or superexchange) or indirect interactions between atoms of neighboring particles, which does not contradicts the concept of the RA model [3, 8], which was used in this study to interpret the results. The presence of a root dependence of exchange constant ($L \propto A_{eff}^{1/2}$) in expression (3) does not exclude the possibility of particle cluster formation because of fairly weak exchange interactions. Note that the obtained estimate of the A_{eff}) value is more than two orders of magnitude smaller than the corresponding constants for bulk ferromagnetic materials.

Table 3. Proportionality between the magnetic moment of a particle, μ_p, and its volume V and size d and proportionality between the dipole-interaction energy E_{dip} (according to expression (A1)) and particle size d for the cases of FM ordering (second column) and AFM ordering (the third, fourth, and fifth columns contain different b values according to the Néel hypothesis (2)

$\mu_p \propto V^b$	$\mu_p \propto V^1$	$\mu_p \propto V^{2/3}$	$\mu_p \propto V^{1/2}$	$\mu_p \propto V^{1/3}$
$\mu_p \propto f(d)$	$\mu_p \propto d^3$	$\mu_p \propto d^2$	$\mu_p \propto d^{3/2}$	$\mu_p \propto d^1$
$E_{dip} \propto f(d)$	$E_{dip} \propto d^3$	$E_{dip} \propto d$	$E_{dip} \propto d^0 \approx$ const	$E_{dip} \propto d^{-1}$

5. CONCLUSIONS

We investigated the dependence of the SPM blocking temperature on external magnetic field, $T_B(H)$, for two samples of nanoferrihydrite powder systems. The analysis of the obtained dependences $T_B(H)$ showed that the classical expression disregarding magnetic interparticle interactions cannot describe the experimentally observed, rather fast decrease in the blocking temperature with an increase in the external field. At the same time, the approach within the RA model [3, 8], which considers clusters of particles with correlated behavior of magnetic moments, not only provides good agreement between the experimental and model dependences $T_B(H)$ but also yields reasonable values of the effective magnetic anisotropy constant.

The correlated behavior of the magnetic moments of particles is a sign of magnetic interparticle interactions; therefore, such interactions play an important and essential role in the magnetic behavior of ferrihydrite nanoparticle systems.

In addition to the aforementioned feature of the functional dependence $T_B(H)$ (fast decrease with an increase in field), magnetic interparticle interactions lead to an increase in the SPM blocking temperature, determined in weak fields. Note that the magnetic anisotropy constants found using the classical Néel–

Brown expression are overestimated several times. Within the used approach based on the RA model, one can obtain the value of magnetic anisotropy constant K_{eff} as a characteristic of noninteracting particles. For the ferrihydrite samples investigated in this work, the K_{eff} values turned out to depend on the particle size, which gives grounds to speak about the contribution of surface magnetic anisotropy and separate the constants corresponding to the volume and surface anisotropy: $K_V \approx 4.7 \times 10^5$ erg/cm^3 and $K_S = 0.09$ erg/cm^2. The performed quantitative estimation of the magnetic-interaction energy exceeds the possible contribution of magnetic dipole–dipole interactions, which is indicative of exchange (direct or indirect) interactions between atoms of neighboring particles in the investigated ferrihydrite systems.

APPENDIX

Estimation of the Energy of Magnetic Dipole–Dipole Interactions for AFM-Nanoparticle Systems

In magnetostatics, the energy of magnetic dipole–dipole interactions E_{dip} for two particles with magnetic moments μ_{p1} and μ_{p2} is determined as

$$E_{dip} = kT_{dip} \approx \mu_{p1}\mu_{p2}/d^3_{p-p}. \quad \text{(A1)}$$

Here, d_{p-p} is the distance between the centers of particles. If particles are of the same size, have the same magnetic moment ($\mu_{p1} = \mu_{p2}$), and are in direct contact (have not any "nonmagnetic" shell), $d_{p-p} = d$. For single-domain FM nanoparticles, $\mu_p \propto V \propto d^3$; then, expression (A1) yields $E_{dip} \propto d^3$. For AFM nanoparticles (the particles are assumed to be of the same size as well), the size dependence of E_{dip} will be determined by the exponent b in expression (2), in which $\mu_{un} \propto N^b \propto V^b$. If $b = 2/3$ and $\mu_{p1,2} = \mu_{un} \propto V^{2/3} \propto d^2$ (the case where a particle has an odd number of ferromagnetically ordered planes [15]), $E_{dip} \propto d$. If $b = 1/3$ and $\mu_{p1,2} = \mu_{un} \propto V^{1/3} \propto d^1$ (the case where μ_{un} is determined by the defects on the particle surface), $E_{dip} \propto d^{-1}$, and the contribution of particle–particle interactions rapidly decreases with an increase in the particle size. Finally, if $b = 1/2$ and $\mu_{p1,2} = \mu_{un} \propto V^{1/2} \propto d^{3/2}$ (μ_{un} is determined by the defects both on the particle surface and in the particle bulk), $E_{dip} \propto d^0 \approx$ const; in other words, the dipole–dipole interaction energy is independent of the particle size. The proportionality types obtained for the cases under consideration are listed in Table 3.

For the systems of ferrihydrite particles characterized by $b \approx 1/2$ and having no organic shell, the influence of magnetic dipole–dipole particle–particle interactions will be identical for samples containing particles of different sizes. Obviously, if we take into account the organic coating of particles in expression (A1) (as well as for sample FH-0h), i.e., substitute $d_{p-p} = d + 2l$ (l is the thickness of organic coating) instead of $d_{p-p} = d$, the E_{dip} value will be smaller for the sample with particles having an organic coating. To perform a quantitative estimation according to expression (A1), it is necessary to take into account the number of nearest neighbors N_N. At $N_N = 12$, $\mu_{p1,2} = \langle\mu_{un}\rangle = 160\mu_B$, $d_{p-p} = \langle d\rangle + 2l$, $\langle d\rangle = 2.7$ nm, and $l = 0.15$ nm, expression (A1) yields $T_{dip} \approx 7$ K for sample FH-0h. For sample FH-24h, at $N_N = 12$, $\mu_{p1,2} = \langle\mu_{un}\rangle = 300\mu_B$, and $d_{p-p} = \langle d\rangle = 3.8$ nm, the T_{dip} value is 12.3 K.

ACKNOWLEDGMENTS

We are grateful to M.N. Volochaev for the microscopy analysis. Electron microscopy studies were performed using equipment of the Center for Collective Use of the Federal Research Center "Krasnoyarsk Science Center of the Siberian Branch of the Russian Academy of Sciences."

FUNDING

This study was supported by the Russian Science Foundation, project no. 22-72-00134.

CONFLICT OF INTEREST

The authors declare that they have no conflicts of interest.

REFERENCES

1. S. Morup, M. F. Hansen, and C. Frandsen, Beilstein J. Nanotechnol. **1**, 182 (2010).
2. D. Caruntu, G. Caruntu, and Ch. J. O'Connor, J. Phys. D: Appl. Phys. **40**, 5801 (2007).
3. M. Knobel, W. C. Nunes, H. Winnischofer, T. C. R. Rocha, L. M. Socolovsky, C. L. Mayorga, and D. Zanchet, J. Non-Cryst. Solids **353**, 743 (2007).
4. M. Knobel, W. C. Nunes, L. M. Socolovsky, E. de Biasi, J. M. Vargas, and J. C. Denardin, J. Nanosci. Nanotechnol. **8**, 2836 (2008).
5. A. M. Pereira, C. Pereira, A. S. Silva, D. S. Schmool, C. Freire, J.-M. Grenche, and J. P. Araujo, J. Appl. Phys. **109**, 114319 (2011).
6. D. A. Balaev, S. V. Semenov, A. A. Dubrovskiy, S. S. Yakushkin, V. L. Kirillov, and O. N. Martyanov, J. Magn. Magn. Mater. **440**, 199 (2017).
7. C. A. M. Vieira, R. Cabreira Gomes, F. G. Silva, A. L. Dias, R. Aquino, A. F. C. Campos, and J. Depeyrot, J. Phys.: Condens. Matter. **31**, 17580 (2019).
8. J. M. Vargas, W. C. Nunes, L. M. Socolovsky, M. Knobel, and D. Zanchet, Phys. Rev. B **72**, 184428 (2005).
9. K. Nadeem, H. Krenn, T. Traussnig, R. Würschum, D. V. Szabø, and I. Letofsky-Papst, J. Magn. Magn. Mater. **323**, 1998 (2011).
10. S. V. Komogortsev, V. A. Fel'k, and O. A. Li, J. Magn. Magn. Mater. **473**, 410 (2011).
11. L. L. Afremov, S. V. Anisimov, and I. G. Iliushin, Chin. J. Phys. **70**, 324 (2021).

12. S. V. Komogortsev, R. S. Iskhakov, and V. A. Fel'k, J. Exp. Theor. Phys. **128**, 754 (2019).
13. S. Morup, D. E. Madsen, C. Fradsen, C. R. H. Bahl, and M. F. Hansen, J. Phys.: Condens. Matter **19**, 213202 (2007).
14. Yu. L. Raikher and V. I. Stepanov, J. Exp. Theor. Phys. **107**, 435 (2008).
15. L. Néel, C. R. Acad. Sci. (Paris) **253**, 203 (1961).
16. A. Millan, A. Urtizberea, N. J. O. Silva, F. Palacio, V. S. Amaral, E. Snoeck, and V. Serin, J. Magn. Magn. Mater. **312**, L5 (2007).
17. P. Dutta, S. Pal, M. S. Seehra, N. Shah, and G. P. Huffman, J. Appl. Phys. **105**, 07B501 (2009).
18. V. L. Kirillov, D. A. Balaev, S. V. Semenov, K. A. Shaikhutdinov, and O. N. Martyanov, Mater. Chem. Phys. **145**, 75 (2014).
19. V. L. Kirillov, S. S. Yakushkin, D. A. Balaev, A. A. Dubrovskiy, S. V. Semenov, Yu. V. Knyazev, O. A. Bayukov, D. A. Velikanov, D. A. Yatsenko, and O. N. Martyanov, Mater. Chem. Phys. **225**, 292 (2019).
20. C. Gilles, P. Bonville, K. K. W. Wong, and S. Mann, Eur. Phys. J. B **17**, 417 (2014).
21. C. Gilles, P. Bonville, H. Rakoto, J. M. Broto, K. K. W. Wong, and S. Mann, J. Magn. Magn. Mater. **241**, 430 (2002).
22. A. Punnoose, T. Phanthavady, M. Seehra, N. Shah, and G. Huffman, Phys. Rev. B **69**, 054425 (2004).
23. N. J. O. Silva, V. S. Amaral, and L. D. Carlos, Phys. Rev. B **71**, 184408 (2005).
24. D. A. Balaev, A. A. Dubrovskii, A. A. Krasikov, S. V. Stolyar, R. S. Iskhakov, V. P. Ladygina, and E. D. Khilazheva, JETP Lett. **98**, 139 (2013).
25. D. A. Balaev, A. A. Krasikov, A. A. Dubrovskii, S. V. Semenov, O. A. Bayukov, S. V. Stolyar, R. S. Iskhakov, V. P. Ladygina, and L. A. Ishchenko, J. Exp. Theor. Phys. **119**, 479 (2014).
26. D. A. Balaev, A. A. Krasikov, A. A. Dubrovskiy, S. I. Popkov, S. V. Stolyar, O. A. Bayukov, R. S. Iskhakov, V. P. Ladygina, and R. N. Yaroslavtsev, J. Magn. Magn. Mater. **410**, 71 (2016).
27. S. V. Stolyar, R. N. Yaroslavtsev, R. S. Iskhakov, O. A. Bayukov, D. A. Balaev, A. A. Dubrovskii, A. A. Krasikov, V. P. Ladygina, A. M. Vorotynov, and M. N. Volochaev, Phys. Solid State **59**, 555 (2017).
28. S. V. Stolyar, D. A. Balaev, A. A. Krasikov, A. A. Dubrovskiy, R. N. Yaroslavtsev, O. A. Bayukov, M. N. Volochaev, and R. S. Iskhakov, J. Supercond. Nov. Magn. **31**, 1133 (2018).
29. Yu. V. Knyazev, D. A. Balaev, S. V. Stolyar, O. A. Bayukov, R. N. Yaroslavtsev, V. P. Ladygina, D. A. Velikanov, and R. S. Iskhakov, J. Alloys Compd. **851**, 156753 (2021).
30. Yu. V. Knyazev, D. A. Balaev, R. N. Yaroslavtsev, A. A. Krasikov, D. A. Velikanov, Yu. L. Mikhlin, M. N. Volochaev, O. A. Bayukov, S. V. Stolyar, and R. S. Iskhakov, Adv. Nano Res. **12**, 605 (2022).
31. D. A. Balaev, A. A. Krasikov, S. V. Stolyar, R. S. Iskhakov, V. P. Ladygina, R. N. Yaroslavtsev, O. A. Bayukov, A. M. Vorotynov, M. N. Volochaev, and A. A. Dubrovskii, Phys. Solid State **58**, 1782 (2016).
32. L. Gutiérrez, V. Barrøn, M. Andrés-Vergés, C. J. Serna, S. Veintemillas-Verdaguer, M. P. Morales, and F. J. Lázaro, J. Geophys. Res. Solid Earth **121**, 4118 (2016).
33. S. V. Stolyar, O. A. Bayukov, V. P. Ladygina, R. S. Iskhakov, L. A. Ishchenko, V. Yu. Yakovchuk, K. G. Dobretsov, A. I. Pozdnyakov, and O. E. Piksina, Phys. Solid State **53**, 100 (2011).
34. B. Vallina, J. D. Rodriguez-Blanco, A. P. Brown, L. G. Benning, and J. A. Blanco, J. Nanopart. Res. **16**, 2322 (2014).
35. E. L. Duarte, R. Itri, E. Lima, Jr., M. S. Baptista, T. S. Berquo, and G. F. Goya, Nanotechnology **17**, 5549 (2006).
36. T. S. Berquo, J. J. Erbs, A. Lindquist, R. L. Penn, and S. K. Banerjee, J. Phys. : Condens. Matter **21**, 176005 (2009).
37. Yu. V. Knyazev, D. A. Balaev, S. V. Stolyar, A. A. Krasikov, O. A. Bayukov, M. N. Volochaev, R. N. Yaroslavtsev, V. P. Ladygina, D. A. Velikanov, and R. S. Iskhakov, J. Alloys Compd. **889**, 161623 (2021).
38. D. A. Balaev, S. V. Stolyar, Yu. V. Knyazev, R. N. Yaroslavtsev, A. I. Pankrats, A. M. Vorotynov, A. A. Krasikov, D. A. Velikanov, O. A. Bayukov, V. P. Ladygina, and R. S. Iskhakov, Results Phys. **35**, 105340 (2022).
39. Yu. V. Knyazev, D. A. Balaev, S. A. Skorobogatov, D. A. Velikanov, O. A. Bayukov, S. V. Stolyar, R. N. Yaroslavtsev, and R. S. Iskhakov, Phys. Rev. B **107**, 115413 (2023).
40. A. A. Krasikov, Yu. V. Knyazev, D. A. Balaev, D. A. Velikanov, S. V. Stolyar, Yu. L. Mikhlin, R. N.Yaroslavtsev, and R. S. Iskhakov, Phys. B (Amsterdam, Neth.) **660**, 414901 (2023).
41. D. A. Velikanov, Vestn. SibGAU **2** (48), 176 (2013).
42. A. D. Balaev, Yu. V. Boyarshinov, M. M. Karpenko, and B. P. Khrustalev, Prib. Tekh. Eksp., No. 3, 167 (1985).
43. J. Zhao, F. E. Huggins, Z. Feng, and G. P. Huffman, Phys. Rev. B **54**, 3404 (1996).
44. S. V. Stolyar, D. A. Balaev, V. P. Ladygina, A. A. Dubrovskiy, A. A. Krasikov, S. I. Popkov, O. A. Bayukov, Yu. V. Knyazev, R. N. Yaroslavtsev, M. N. Volochaev, R. S. Iskhakov, K. G. Dobretsov, E. V. Morozov, O. V. Falaleev, E. V. Inzhevatkin, et al., J. Supercond. Nov. Magn. **31**, 2297 (2018).
45. J. Fock, M. F. Hansen, C. Frandsen, and S. Morup, J. Magn. Magn. Mater. **445**, 11 (2018).
46. E. M. Chudnovsky, W. M. Saslow, and R. A. Scrota, Phys. Rev. B **33**, 251 (1986).
47. J. C. Denardin, A. L. Brandl, M. Knobel, P. Panissod, A. B. Pakhomov, H. Liu, and X. X. Zhang, Phys. Rev. B **65**, 064422 (2002).
48. D. A. Balaev, S. I. Popkov, A. A. Krasikov, A. D. Balaev, A. A. Dubrovskii, S. V. Stolyar, R. N. Yaroslavtsev, V. P. Ladygina, and R. S. Iskhakov, Phys. Solid State **59**, 1940 (2017).
49. A. A. Krasikov and D. A. Balaev, J. Exp. Theor. Phys. **136**, 97 (2023).
50. A. Aharoni, J. Appl. Phys. **61**, 3302 (1987).

51. F. Bodker, S. Morup, and S. Linderoth, Phys. Rev. Lett. **72**, 282 (1994).
52. J. Mohapatra, M. Xing, J. Elkins, J. Beatty, and J. Ping Liu, J. Phys. D: Appl. Phys. **53**, 504004 (2020).
53. D. A. Balaev, I. S. Poperechny, A. A. Krasikov, S. V. Semenov, S. I. Popkov, Y. V. Knyazev, V. L. Kirillov, S. S. Yakushkin, O. N. Martyanov, and Yu. L. Raikher, J. Phys. D: Appl. Phys. **54**, 275003 (2021).
54. R. D. Zysler, M. Vasquez Mansilla, and D. Fiorani, Eur. Phys. J. B **41**, 171 (2004).
55. M. P. Proenca, C. T. Sousa, A. M. Pereira, P. B. Tavares, J. Ventura, M. Vazquez, and J. P. Araujo, Phys. Chem. Chem. Phys. **13**, 9561 (2011).
56. X. Batlle and A. Labarta, J. Phys. D: Appl. Phys. **35**, R15 (2002).
57. C.-R. Lin, R.-K. Chiang, J.-S. Wang, and T.-W. Sung, J. Appl. Phys. **99**, 08N710 (2006).
58. Yu. V. Knyazev, D. A. Balaev, V. L. Kirillov, O. A. Bayukov, and O. N. Mart'yanov, JETP Lett. **108**, 527 (2018).

Translated by Yu. Sin'kov